Single Relaxation Time and Multiple Revised Matrix Lattice Boltzmann Simulations of Forced Isotropic Turbulence

Waleed Abdel Kareem[1,2], Pietro Asinari[3], Sauro Succi[4], Seiichiro Izawa[5], Yu Fukunishi[6]
[1]*Department of Mathematics, Faculty of Science, Suez University, Egypt*
[2]*Academy of Scientific Research & Technology, Egypt*
[3]*Politecnico di Torino - Department of Energy, Corso Duca degli Abruzzi, 24, 10129, Torino (Italy)*
[4]*Instituto Applicazioni Calcolo CNR, Italy*
[5]*Department of Mechanical Engineering and Sciences, University of Toyama, Japan*
[6]*Institute of Computational Fluid Dynamics, Japan*
**Corresponding author: waleed.abdelkareem@sci.suezuni.edu.eg*

Abstract

The single relaxation time (SRT) and the revised matrix (RM) lattice Boltzmann models are compared for simulations of three dimensional forced isotropic turbulence with resolutions of 128^3 and 256^3, respectively. The forcing technique by Guo *et al.* (2002) is applied with the two models using the same parameters and conditions. Some new aspects and results have been confirmed such as the superiority of the MRT model to simulate forced turbulence and using the Courant-Friedichs-Lewy condition (CFL) (Courant *et al.*, 1967) by multiplying the velocity input with the coefficient CFL < 1.0 to overcome the stability problem and divide the output velocity data by the same CFL. The initial velocity field is chosen as $\mathbf{u}(\mathbf{x}, 0) = 0$ and the force is injected at low wave-numbers with a fixed forcing amplitude to 10^{-4} for all cases. The single relaxation time is set to $\tau = 0.503$ in all SRT simulations. Results show that the obtained turbulent velocity fields yield universal characteristics as proven in previous theoretical, experimental and numerical studies. The Taylor Reynolds number for the simulations are found as SRT: $R_\lambda = 62$ and $MRT: R_\lambda = 65$ for 128^3 and SRT: $R_\lambda = 107$ and MRT: $R_\lambda = 82$ for the case of 256^3, respectively. To test the weak incompressibility for the SRT model in comparison to the MRT model, the density probability distribution function (PDF) is depicted and it is found that ρ is almost unity at all timesteps for the MRT case, while a clear disturbance about unity is observed for the SRT case. Time variation's statistics such as the Taylor Reynolds number R_λ, the Taylor microscale λ, the Kolmogrov microscale η and energy spectra are calculated and depicted for all cases. One of the disadvantages of the MRT case is the simulations time which is found about twice the SRT simulations time, where about 80 hours are needed for simulating 12000 timesteps in the 256^3 case in comparison to 42 hours for the SRT model using the same hardware resources.

Keywords: Lattice Boltzmann; SRT and MRT; Vortical structures; Energy spectrum; Velocity PDF.

1. Introduction

Simulations of forced turbulence using the spectral method to solve the Navier-Stokes equations are studied widely and many interesting results were obtained. It was found that in isotropic turbulence, the flow is fully filled by elongated tube-like vortical structures and the velocity spectra follow the Kolmogrov $-5/3$ power law. Direct numerical simulations of homogeneous isotropic turbulence using Fourier spectral method with resolutions up to 4096^3 and Taylor Reynolds number up to 1201 have been performed on the earth simulator by Yokokawa *et al.* (2002); Kaneda *et al.* (2003). Their datasets suggest that the

normalized mean energy dissipation becomes independent of the kinematic viscosity. Also, they reported that the scaling of the energy spectrum is about 0.1 steeper than the Kolmogrov scaling. Some other studies was devoted to investigate the characteristics of homogeneous isotropic turbulence such as Vincent and Menequzzi (1991) and others. Those studies were also performed numerically using the spectral method to solve the Navier-Stokes equations and their visualization of the flow field confirmed the existence of very elongated worm-like structures. Their results suggest that the energy spectrum in the inertial sub-range follows the $k^{-5/3}$ Kolmogorov power scaling law where k is the wave number.

In the last few years, the lattice Boltzmann method (LBM) is highly developed and has become a powerful method for simulations of different fluid dynamics problems. The LBM is widely applied in simulations of complex fluid flows such as cavity flow, multiphase flow and other engineering problems. Simulations of forced homogeneous and isotropic turbulent flows are not popular because adding the force to the LBM is still under development due to the stability issue and the nature of the method. In a recent study (Waleed *et al.*, 2022a), the forcing function and its amplitude, initialization of the flow field, the injection cutoff wavenumber, and the relaxation time are carefully chosen to strength the stability process at several resolutions and with different forcing functions. Also, comparison between the variable forcing techniques of the lattice Boltzmann method for simulations of box turbulent is discussed in Waleed *et al.* (2022b) with resolutions of 128^3 and 256^3, respectively. The decaying turbulent flow is investigated using the different lattice Boltzmann models such as the recent study of Haussmann *et al.* (2019) which is devoted for investigating the stability, consistency and accuracy of LBM. Lall *et al.* (2021) study the derivation of lattice Boltzmann equation from the well known Boltzmann equation, where the mathematical theory behind the lattice Boltzmann equation with its relevant properties is considered and the most important lattice Boltzmann models are examined. Jiang *et al.* (2022) studied the parallel fully resolved simulations for settling suspensions, where it is performed on multiple CPU cores based on the boundary-thickening direct forcing immersed boundary with incompressible lattice Boltzmann models. A high-order lattice Boltzmann method with implicit-explicit flux reconstruction is proposed by Ma *et al.* (2022) for simulating viscous incompressible flows. They introduced a solution of the discrete velocity Boltzmann equation using a high-order flux reconstruction scheme (FR) for spatial discretization. But for the time discretization, they applied a high-order implicit-explicit Runge-Kutta scheme in the generalized curvilinear coordinates with uniform and non-uniform grids. To decrease memory size and to achieve numerical stability for high Rayleigh number thermal flows, the simplified thermal lattice Boltzmann method is introduced by Lu *et al.* (2022). Also, the single and multiple lattice Boltzmann methods are applied to incompressible laminar flow with high Reynolds numbers with a range of $200 - 2000$ for determining stability limits of the single relaxation time (LBM-SRT) and the multiple relaxation time (LBM-MRT)(Aslan *et al.*, 2014) where they analyzed the lid driven cavity flow example.

Despite of such great efforts and efficient developments, some research topics and applications need to be reconsidered because of its importance and lack of references. Some of these topics such as simulations of forced turbulence using different techniques and comparisons between the results of SRT and MRT models. Injection of a force term to the LBM at every time step faces some stability problems in the single relaxation lattice Boltzmann models. So, the objective of this study is to compare the single relaxation time (SRT) model and the multiple relaxation time (MRT) model in simulating forced turbulence using the forcing technique of Guo *et al.* (2002). In the literatures, few forcing techniques of the lattice Boltzmann equation are introduced and it will be discussed in detail in the forcing section (Kupershtokh, 2004; Mohamad and Kuzmin, 2010). For example, Buick and Greated (2000); Guo *et al.* (2002) used the Poiseuille flow problem in testing the LBM forcing difficulties and stability. Mohamad and Kuzmin (2010) examined the forcing of the LBM on the study of the natural convection problem in an open ended cavity as ideal candidate. For isotropic turbulence, Waleed *et al.* (2006, 2009) applied the forcing method to the SRT for simulating box turbulence with resolutions of 128^3 and 256^3, respectively. There are several techniques for forcing the lattice Boltzmann equation, the first technique is depending on shifting the velocity field based on the Newtonian 2^{nd} law, the second techniques is depending on adding the force at the collision term as a special term where it was previously proposed by Waleed *et al.* (2009). The third technique considered the velocity shifting and adding the force to the collision process

at the same time. The fourth technique is taking into account the discrete lattice effects on the forcing as discussed by Guo *et al.* (2002). In previous efforts, the LBM with a constant external force are investigated in studying different fluid problems such as box turbulence (Waleed *et al.*, 2009; Cate *et al.*, 2006), where the energy spectrum has a $k^{-5/3}$ Kolmogorov scaling law in the inertial sub-range (k is the wave-number). The same forcing function that is introduced by Waleed *et al.* (2009) has been used in some recent studies such as studying the thermodynamics of a real fluid (Albernaz *et al.*, 2016) and investigating the single droplet in isotropic turbulence using numerical simulations with a hybrid lattice Boltzmann scheme (Albernaz *et al.*, 2017).

The SRT model stability and accuracy were argued by many researchers during their applications and hence there are many efforts to overcome such drawbacks. One of the important development is to use the multiple relaxation time (MRT) lattice Boltzmann model. The MRT lattice Boltzmann equation overcomes some defects of the SRT models such as fixed Prandtl number and fixed ratio between the kinematic and bulk viscosities. A rapid development of the MRT has been observed in the last few years. Developments include formulation of optimal boundary conditions (Ginzbourg and Adler, 1994; Ladd, 1994), viscoelastic models (Giraud, 1997a,b) and models with reduced lattice symmetries (d'Humeres *et al.*, 2001; Bouzidi-1 *et al.*, 2001a). Lallemand and Luo (2000) show that MRT-LBE models are much more stable than their LBGK counterparts. They demonstrate the superior stability of MRT-LBE to the lattice Bhatnager-Gross-Krook (LBGK) (Bhatnagar *et al.*, 1954) where they studied the three-dimensional cavity flow and comparisons with the results of the LBGK are also considered in their study .

In this paper, the matrix lattice Boltzmann is tested in simulations of forced isotropic turbulence which is a standard candidate in turbulence studies and the results are compared to the SRT for resolutions of 128^3 and 256^3. This paper is organized as follows. Section 2 discusses the SRT and MRT lattice Boltzmann models. Discussions about the different forcing methods and the present forcing applications are considered in section 3. Section 4 is devoted to the results of the study with comparisons with previous efforts of the SRT model and the Fourier spectral method. Section 5 summarizes the conclusion.

2. SRT and Revised Matrix $D3Q19$ lattice Boltzmann model

2.1 The SRT lattice Boltzmann model

The single relaxation time model can be represented by the following equation:

$$\begin{aligned} & f_\alpha(\boldsymbol{x}+\boldsymbol{e}_\alpha\delta t, t+\delta t) - f_\alpha(\boldsymbol{x},t) \\ & \quad = \frac{-1}{\tau}(f_\alpha(\boldsymbol{x},t) - f_\alpha^{eq}(\boldsymbol{x},t)) + \Delta t F_i. \end{aligned} \tag{1}$$

The relaxation time τ is one of the main parameters for LB simulations when an additional force term ($\Delta t F_i$) is added to the collision term $\frac{-1}{\tau}(f_\alpha(\boldsymbol{x},t) - f_\alpha^{eq}(\boldsymbol{x},t))$. The different parameters in Eqn.1 are defined as follows; the $19-$particle velocities e_α are defined by

$$\boldsymbol{e}_\alpha = \begin{cases} (0,0,0), & \alpha = 0 \\ (\pm1,0,0),(0,\pm1,0),(0,0,\pm1), & \alpha = 1-6 \\ (\pm1,\pm1,0),(\pm1,0,\pm1),(0,\pm1,\pm1), & \alpha = 7-18 \end{cases},$$

and the weighting coefficients w_α that are calculated from the conservation laws for the $19-$particles are

$$w_\alpha = \begin{cases} \frac{1}{3}, & \alpha = 0 \\ \frac{1}{18}, & \alpha = 1-6 \\ \frac{1}{36}, & \alpha = 7-18 \end{cases}.$$

The function $f_\alpha(\boldsymbol{x},t)$ in Eqn.1 represents the distribution function or the fluid density at a point x and at a time t that is moving with the velocity e_α per time step, then with time advancement the distribution function will be updated to $f_\alpha(\boldsymbol{x}+\boldsymbol{e}_\alpha\delta t, t+\delta t)$. Also, from Eqn.1; $f_\alpha^{eq}(\boldsymbol{x},t)$ is the equilibrium distribution function and it is defined as

$$f_\alpha^{eq}(\boldsymbol{x},t) = w_\alpha\rho[1 + 3(\boldsymbol{e}_\alpha.\boldsymbol{u}) + \frac{9}{2}(\boldsymbol{e}_\alpha.\boldsymbol{u})^2 - \frac{3}{2}(\boldsymbol{u}.\boldsymbol{u})]. \tag{2}$$

The different macroscopic quantities are derived from the updated distribution function at every time step (such as the fluid density $\rho = \sum_\alpha f_\alpha$ and the fluid velocity $u = \frac{1}{\rho}\sum_\alpha e_\alpha f_\alpha$). It is important to note that, the velocity fields as well as the fluid density are saved at every output file to discuss the incompressibility for the SRT and MRT models.

2.2 RM lattice Boltzmann model

The evolution equation of the MRT lattice Boltzmann equation (Humeres, 1992; d'Humieres *et al.*, 2002) can be written as

$$|f(\boldsymbol{x}+\boldsymbol{v},t+1)\rangle - |f(\boldsymbol{x},t)\rangle = -M^{-1}\hat{S}\left[|m(\boldsymbol{x},t)\rangle - |m^{eq}(\boldsymbol{x},t)\rangle\right], \tag{3}$$

where the collision matrix $\hat{S} = M \cdot S \cdot M^{-1}$ is diagonal and m_α^{eq} is the equilibrium value of the moment m_α. More details about the collision matrix and other variables can be found in (d'Humieres *et al.*, 2002). In this paper, the revised matrix lattice Boltzmann (RM) that was introduced by Karlin *et al.* (2011) is used in the simulations. The method was introduced to enhance stability and keep the simplicity of the LBGK model (Bhatnagar *et al.*, 1954). The method is based on two-step relaxation BGK-like collision operator, in which the two time-scales describe relaxation to two distinct equilibria, one of which is the fixed point of the relaxation and the other is an intermediate state. Karlin *et al.* (2011) suggested a two-parametric family of lattice Boltzmann equations based on an intermediate state of relaxation f^C,

$$f(\boldsymbol{x}+\boldsymbol{v},t+1) - f(\boldsymbol{x},t) = -\omega_1(f - f^C) - \omega_2(f^C - f^{eq}), \tag{4}$$

where, f^{eq} represents the local equilibrium distribution which depends on the local density ρ and $\rho\boldsymbol{u} = \langle \boldsymbol{v} f\rangle$. Her, $\boldsymbol{u}$ is the local flow velocity and $\langle ...\rangle$ denotes a sum over the discrete velocity $\boldsymbol{v}_i$,$i = 1, ...19$. $f(\boldsymbol{x},t)$ is a vector of populations f_i corresponding to the discrete velocities $\boldsymbol{v}_i$ at the site $\boldsymbol{x}$ and time t. Equation 4 can be written in the LBGK-like form

$$f(\boldsymbol{x}+\boldsymbol{v},t+1) - f(\boldsymbol{x},t) = -\omega_1(f - f^{GE}), \tag{5}$$

where the generalized equilibrium f^{GE} is defined as

$$f^{GE} = \frac{\omega_2}{\omega_1} f^{eq} + (1 - \frac{\omega_2}{\omega_1}) f^C. \tag{6}$$

More details about the method and properties of the intermediate function f^C can be found in Karlin *et al.* (2011). The $D3Q19$ generalized equilibrium f^{GE} can be respectively written as

$$\begin{aligned}
f^{GE}_{(0,0,0)} &= \rho(1 - S^{eq}_{xx} - S^{eq}_{yy} - S^{eq}_{zz} + S^{eq}_{xx}S^{eq}_{yy} + S^{eq}_{yy}S^{eq}_{zz} + S^{eq}_{xx}S^{eq}_{zz}) \\
f^{GE}_{(+1,0,0)} &= \frac{\rho}{2}(1 - S^{eq}_{yy} - S^{eq}_{zz})S^{eq}_{xx} + u_x - (u_x S^{eq}_{yy} + u_x S^{eq}_{zz}) \\
f^{GE}_{(-1,0,0)} &= \frac{\rho}{2}(1 - S^{eq}_{yy} - S^{eq}_{zz})S^{eq}_{xx} - u_x + (u_x S^{eq}_{yy} + u_x S^{eq}_{zz}) \\
f^{GE}_{(0,+1,0)} &= \frac{\rho}{2}(1 - S^{eq}_{xx} - S^{eq}_{zz})S^{eq}_{yy} + u_y - (u_y S^{eq}_{xx} + u_y S^{eq}_{zz}) \\
f^{GE}_{(0,-1,0)} &= \frac{\rho}{2}(1 - S^{eq}_{xx} - S^{eq}_{zz})S^{eq}_{yy} - u_y + (u_y S^{eq}_{xx} + u_y S^{eq}_{zz}) \\
f^{GE}_{(0,0,+1)} &= \frac{\rho}{2}(1 - S^{eq}_{xx} - S^{eq}_{yy})S^{eq}_{zz} + u_z - (u_z S^{eq}_{yy} + u_z S^{eq}_{xx}) \\
f^{GE}_{(0,0,-1)} &= \frac{\rho}{2}(1 - S^{eq}_{xx} - S^{eq}_{yy})S^{eq}_{zz} - u_z + (u_z S^{eq}_{yy} + u_z S^{eq}_{xx}) \\
f^{GE}_{(+1,+1,0)} &= \frac{\rho}{4}(S^{eq}_{xx}S^{eq}_{yy} + u_x u_y + u_x S^{eq}_{yy} + u_y S^{eq}_{xx}) \\
f^{GE}_{(+1,-1,0)} &= \frac{\rho}{4}(S^{eq}_{xx}S^{eq}_{yy} - u_x u_y + u_x S^{eq}_{yy} - u_y S^{eq}_{xx}) \\
f^{GE}_{(-1,+1,0)} &= \frac{\rho}{4}(S^{eq}_{xx}S^{eq}_{yy} - u_x u_y - u_x S^{eq}_{yy} + u_y S^{eq}_{xx})
\end{aligned}$$

$$
\begin{aligned}
f^{GE}_{(-1,-1,0)} &= \frac{\rho}{4}(S^{eq}_{xx}S^{eq}_{yy} + u_x u_y - u_x S^{eq}_{yy} - u_y S^{eq}_{xx}) \\
f^{GE}_{(0,+1,+1)} &= \frac{\rho}{4}(S^{eq}_{zz}S^{eq}_{yy} + u_z u_y + u_z S^{eq}_{yy} + u_y S^{eq}_{zz}) \\
f^{GE}_{(0,+1,-1)} &= \frac{\rho}{4}(S^{eq}_{zz}S^{eq}_{yy} - u_z u_y - u_z S^{eq}_{yy} + u_y S^{eq}_{zz}) \\
f^{GE}_{(0,-1,+1)} &= \frac{\rho}{4}(S^{eq}_{zz}S^{eq}_{yy} - u_z u_y + u_z S^{eq}_{yy} - u_y S^{eq}_{zz}) \\
f^{GE}_{(0,-1,-1)} &= \frac{\rho}{4}(S^{eq}_{zz}S^{eq}_{yy} + u_z u_y - u_z S^{eq}_{yy} - u_y S^{eq}_{zz}) \\
f^{GE}_{(+1,0,+1)} &= \frac{\rho}{4}(S^{eq}_{zz}S^{eq}_{xx} + u_z u_x + u_x S^{eq}_{zz} + u_x S^{eq}_{zz}) \\
f^{GE}_{(+1,0,-1)} &= \frac{\rho}{4}(S^{eq}_{zz}S^{eq}_{xx} - u_z u_x - u_x S^{eq}_{zz} + u_x S^{eq}_{zz}) \\
f^{GE}_{(-1,0,+1)} &= \frac{\rho}{4}(S^{eq}_{zz}S^{eq}_{xx} - u_z u_x + u_x S^{eq}_{zz} - u_x S^{eq}_{zz}) \\
f^{GE}_{(-1,0,-1)} &= \frac{\rho}{4}(S^{eq}_{zz}S^{eq}_{xx} + u_z u_x - u_x S^{eq}_{zz} - u_x S^{eq}_{zz}). \qquad (7)
\end{aligned}
$$

Here $S^{eq}_{\alpha\alpha} = c_s^2 + u_\alpha^2$ and $c_s^2 = \frac{1}{3}$ and u_x, u_y, u_z are the three velocity components. Equations 5 and 7 represent the revised matrix model that will be used in this study to generate the velocity fields with a constant forcing at each time step. The simulations have been done in periodic boxes with dimensions of 128^3 and 256^3, respectively.

3. Forcing method

Different types of forcing schemes have been developed for isotropic turbulent flow simulations. The Fourier spectral method is used to solve such types of flows in Fourier domain and hence spectral forcing is suitable for such studies. The body force is defined at low wave numbers and imposed on the flow field. Cate *et al.* (2006) combined the spectral forcing with lattice Boltzmann simulations of turbulent flows and they demonstrated that the lattice-Boltzmann method provides a good alternative as a numerical method for direct simulation of forced isotropic turbulence. Some other ideas for forcing the lattice Boltzmann are introduced and they will be discussed in the following three points.

- Luo (1993) suggested the force term $F_i = -3w_i\rho \boldsymbol{e}_i \cdot \boldsymbol{F}/c^2$ to be introduced to the collision term.
- Shan and Chen (1994) proposed that the force term can be added as $F_i = -3w_i(\frac{\boldsymbol{c}_i - \boldsymbol{u}}{c^2} + \frac{\boldsymbol{c}_i - \boldsymbol{u}}{c^4}\boldsymbol{c}_i) \cdot \boldsymbol{F}$.
- Buick and Greated (2000) introduced a modified method where they added the force term $F_i = \frac{4}{c^2}(1 - \frac{1}{2\tau})\boldsymbol{F} \cdot \boldsymbol{c}_i$ to the collision operator and they shifted the equilibrium velocity as $\boldsymbol{u}(\boldsymbol{x}, t) = \frac{1}{\rho}\sum_i \boldsymbol{c}_i f_i(\boldsymbol{x}, t) + \frac{\boldsymbol{F}\Delta t}{2\rho}$
- The velocity field can be shifted, based on newton's second law, as $\boldsymbol{u}(\boldsymbol{x}, t) = \frac{1}{\rho}\sum_i \boldsymbol{c}_i f_i(\boldsymbol{x}, t) + \frac{\boldsymbol{F}_\tau}{\rho}$. without adding a forcing term into the collision operator.
- Guo *et al.* (2002) used the same process by adding a forcing term to the collision operator as

$$
F_i = w_i(1 - \frac{1}{2\tau})(\frac{\boldsymbol{e}_i - \boldsymbol{u}}{c_s^2} + e_i\frac{\boldsymbol{e}_i \cdot \boldsymbol{u}}{c_s^4}\boldsymbol{e}_i) \cdot \boldsymbol{F}, \qquad (8)
$$

  and the fluid velocity defined by $\rho\boldsymbol{u}(\boldsymbol{x}, t) = \sum_i \boldsymbol{e}_i f_i(\boldsymbol{x}, t) + \frac{\Delta t}{2}\boldsymbol{F}$.

Guo *et al.* (2002) introduced this representation of the forcing term to consider the discrete lattice effects. With this representation, the derivation of the Navier-Stokes equation from the lattice Boltzmann equation was performed through the Chapman-Enskog expansion. In this study, the Guo-method (Guo *et al.*,

2002) is used with the SRT and MRT models, respectively. The three components of the forcing function $\boldsymbol{F}$ which is used in this study can be written as Waleed *et al.* (2022a)

$$\boldsymbol{F} \equiv \begin{cases} F_x = A\sum_{k_i=-k_{max}}^{k_{max}} \frac{k_2 k_3}{|\boldsymbol{k}|}\cos(\frac{2\pi}{N}r+\phi) \\ F_y = -2A\sum_{k_i=-k_{max}}^{k_{max}} \frac{k_1 k_3}{|\boldsymbol{k}|}\cos(\frac{2\pi}{N}r+\phi), \\ F_z = A\sum_{k_i=-k_{max}}^{k_{max}} \frac{k_1 k_2}{|\boldsymbol{k}|}\cos(\frac{2\pi}{N}r+\phi) \end{cases}$$

where A and ϕ are the amplitude and the random phase, respectively (Waleed *et al.*, 2006). The forcing amplitude is chosen as 10^{-4} with a low cutoff wave-number ($0 <\mid \boldsymbol{k} \mid\leq 3$) where $\mid \boldsymbol{k} \mid = \sqrt{k_1^2+k_2^2+k_3^2}$. The parameters in the force function are $N = 128$ or $N = 256$ for the two simulations and $r = \boldsymbol{k}\cdot\boldsymbol{x} = (k_1x + k_2y + k_3z)$.

The generalized distribution functions f^{GE} will be changed because the velocities u_x, u_y, u_z and the function $S_{\alpha\alpha}$ will be changed according to the additional forcing term. Some important points for the simulations can be summarized as follows:

- The initial velocity field for the two resolutions are chosen as $\boldsymbol{u}(\boldsymbol{x}, 0) = 0$
- The Courant-Friedichs-Lewy condition(CFL ≤ 1) (Courant *et al.*, 1967) is applied and the velocity input is multiplied by CFL and the output velocity compensation is considered by division of the velocity by CFL. This may help in improving the stability of the LBM simulations.
- The forcing amplitudes are also the same for SRT and MRT simulations.
- The force is injected randomly every time step using a system Gaussian random number generator.

4. Results and discussions

Many statistical features are characterizing turbulent flow such as the Taylor Reynolds number, Taylor micro-scale, Kolmogrov micro-scale, Energy spectrum, skewness, flatness and vortical motion. These features are well established mathematically, estimated and their values are proved by many theoretical and numerical studies. The standard Fourier spectral method is usually used to solve the Navier-Stokes equations for forced turbulence and it can be considered as the main basic reference to other numerical methods. Comparisons of the present turbulent characteristics for the SRT and MRT models to the spectral method results are important and of great interest. Such comparisons can give information about the ability and stability of the LBM models in simulations of forced turbulence. The mathematical definitions for the turbulent parameters will be given. The energy spectrum function $E(\boldsymbol{k})$ at the scalar wave number $k \equiv (\mathbf{k}\cdot\mathbf{k})^{\frac{1}{2}}$ is defined in wavenumber space as

$$E(\boldsymbol{k}) = \frac{1}{2}\sum_{k-\frac{1}{2}<|k|\leq k+\frac{1}{2}} \mid \hat{u}^2(k) \mid, \tag{9}$$

where $\hat{u}$ are the velocity Fourier coefficients. The Taylor Reynolds number R_λ, the Kolmogrov microscale η, the Taylor microscale λ and the energy dissipation rate ϵ are defined respectively as

$$R_\lambda = \frac{u_{rms}\lambda}{\nu}, \tag{10}$$

$$\eta = (\frac{\nu^3}{\epsilon})^{\frac{1}{4}}, \tag{11}$$

where $u_{rms} = \frac{2}{3}\int_0^{k_{max}} E(k)dk$ is the velocity root mean square and ν is the kinematic viscosity.

$$\lambda = \sqrt{\frac{15u_{rms}^2}{S_{ij}S_{ij}}}, \tag{12}$$

and

$$\epsilon = 2\nu S_{ij}S_{ij}. \tag{13}$$

4.1 Statistical results

The flow field is initialized with a null velocity field and the simulations extends to 12000 timesteps with 60 output files for each simulation and for each resolution. Every output file needs about 4.5 minutes using Core i7 computer with speed 3.4 GHz and 12 GB RAM with a total time about 270 minutes for the 128^3-SRT case. The Guo forcing application has been compared for the SRT model with other forcing methods in a previous work (Waleed *et al.*, 2022b). But in this study, some points are different such as the comparison is against the MRT revised matrix model and the fluid density is saved with the velocity for studying the LBM weak incompressibility in SRT and MRT cases. The MRT simulation time for the 128^3 case is found as 10 minutes for each output file which is twice the SRT simulation time. The total consuming time is found as 600 minutes. For the case of 256^3 the SRT simulation time is found as 42 minutes for each output timestep with a total of 42 hours for the 60 output files. In the MRT case the simulation time is found about 80 minutes for each output file with a total time of about 80 hours.

Fig.1 shows the time development of R_λ for the SRT and MRT resolutions, where it can be found that for the case of 128^3, the values for R_λ are between 60 and 80, however for the case of 256^3, the values are about 100 and 120 for the last $20-$timesteps which are reasonable for such resolutions . The time development of the Kolmogrov microscale η is shown in Fig.2, where it is very close to 0.02 for the last 20-timesteps. Also the curve of $k_{max}\eta$ is shown in Fig.3, where it is clear that for the case of 128^3 both of SRT and MRT results are greater than unity for the last 20-timesteps. Also, for the 256^3 case, both of SRT and MRT results are close to 2, which is a good indicator for resolving small scale flows. The figures indicate that the flow field reaches a steady state where most important statistical values oscillates about a constant value at the last 20-timesteps. Fig.4 shows an important result for the density distribution for SRT and MRT results. This figure indicates that the MRT model is superior to the SRT model because incompressibility is better in comparison to the SRT model, where the density almost close to unity. Fig.5 shows the energy spectrum for all cases in this study and it is clear that the MRT spectrum curve are enhanced in comparison to than the SRT results at large wavenumbers where more small scale vortices can be found.

4.2 Visualization of the flow fields

The visualization of the vortical structures in turbulence studies is an important technique to understand the turbulent flow motion. There are many mathematical definitions that can identify the vortical regions of the flow field and several studies compared these definitions such as Waleed2021 (2020); Hunt *et al.* (1998). The high rotational method namely, the $Q-$ identification method (Hunt *et al.*, 1998) can be defined as

$$Q = \frac{1}{2}(\Omega_{ij}\Omega_{ij} - S_{ij}S_{ij}), \tag{14}$$

where $S_{ij}S_{ij}$ represents the strength of the symmetric strain rate tensorS_{ij} and $\Omega_{ij}\Omega_{ij}$ is the strength of the skew symmetric rate of rotation tensor Ω_{ij} and they are defined respectively as

$$S_{ij} = \frac{1}{2}(\frac{\partial u_i}{\partial x_j} + \frac{\partial u_j}{\partial x_i}) \tag{15}$$

and

$$\Omega_{ij} = \frac{1}{2}(\frac{\partial u_i}{\partial x_j} - \frac{\partial u_j}{\partial x_i}). \tag{16}$$

The $Q-$ identification method is used in this study to visualize the flow fields of the simulations. It should be pointed that the visualization thresholds will be normalized by the average enstrophy $< Q_W >$, where $Q_W = \frac{1}{2}\Omega_{ij}\Omega_{ij}$. Figure 6 shows the vortical structures for the case of 128^3-SRT and figure 7 shows the results for the 128^3-MRT case, where many vortices are visualized using the $Q-$identification method at threshold values of $\frac{Q}{Q_W}$ = 5.0. The visualization of tube-like vortices in the cases 256^3-SRT and MRT-256^3 are shown in Fig.8 and Fig.9, respectively. The visualization threshold values are also chosen to be $\frac{Q}{Q_W}$ = 5.0.

4.3 Comparison with Navier-Stokes results

Table 1 shows the comparison between the statistical values of the present study for the SRT and MRT models against the Navier-Stokes published results. The Taylor Reynolds number R_λ is found about 77 for the 128^3-SRT and $R_\lambda = 77$ for the 128^3-MRT which is in good agreement with the studies of Kaneda *et al.* (2003); Vincent and Menequzzi (1991); Jimenez *et al.* (1993); Comete0Bellot and Corrsin (1971); Ooi *et al.* (1999)), where it was reported that the Taylor Reynolds number for simulations with a resolution of 128^3 is of the order of 100.

Table 1. Statistical features of the turbulent field (Resolution 128^3).

	Present study(MRT-D3Q19)	SRT-D3Q19 (Waleed *et al.*, 2009)	SM (Jimenez *et al.*, 1993)
R_λ	65	82	61.1
λ	0.34	0.34	0.5269
η	0.021	0.019	0.016
$k_{max}\eta$	1.34	1.21	2.0

For the 256^3 cases, it is clear that λ, η and $k_{max}\eta$ are close to the previous Navier-Stokes results as shown in table 2.

The skewness S_i and the flatness FT_i of the velocity derivatives are also important variables because they have some universal values in isotropic turbulence, and they are defined as

$$S_i = \frac{< \frac{\partial u_i}{\partial x_i} >^3}{< (\frac{\partial u_i}{\partial x_i})^2 >^{\frac{3}{2}}} , \tag{17}$$

and

$$FT_i = \frac{< \frac{\partial u_i}{\partial x_i} >^4}{< (\frac{\partial u_i}{\partial x_i})^2 >^2} . \tag{18}$$

The velocity derivatives skewness and flatness for the two simulations as well as the isotropic ratio are estimated and they are shown in table 3. The magnitudes of the skewness and flatness values are found similar to the results obtained by the spectral method(SM) where the skewness values are found close to 0.4 which is similar to the spectral methods results as well as the single relaxation lattice Boltzmann efforts (Hazi *et al.*, 2010). Also the flatness values are found close to 4.13 which are also close to the SM results specially in the case of the 256^3 results.

Table 2. Statistical features of the turbulent field (Resolution 256^3).

	Present study(MRT-D3Q19)	SRT-D3Q19 (Waleed *et al.*, 2009)	SM (Jimenez *et al.*, 1993)
R_λ	82	107	167
λ	0.24	0.31	0.203
η	0.0137	0.015	0.007
$k_{max}\eta$	1.75	1.91	0.847

Table 3. Skewness, flatness and isotropic ratios.

	Skewness	Flatness	$\frac{1}{3}\sum I_i$
128^3-SRT	0.396	4.13	1.0
128^3-MRT	0.41	4.69	1.0
256^3-SRT	0.43	6.24	1.0
256^3-MRT	0.44	4.7	1.0

The isotropy ratios of the velocity are defined as $I_i = \frac{3<u_i^2>}{q^2}$, where $q^2(t)= 2\int_0^\infty E(k,t)dt$. The summations of the isotropy ratios are always unity which are in good agreement with previous studies. The velocity density functions (PDFs) for the SRT and MRT simulations are shown in Figs.10 and 11, respectively. The PDFs are shown in a semi-log curve. It is clear that the velocity PDFs in the two cases have a similar behavior to the previous published work specially for the MRT results.

5. Conclusion

Simulations of forced isotropic turbulence with resolutions of 128^3 and 256^3 were carried out using the SRT and the revised matrix lattice Boltzmann $D3Q19$ models. The superiority of the MRT model to the SRT model to simulate forced turbulence with enhanced stability and accuracy was demonstrated using the velocity and density statistics and their PDFs profiles. Some turbulent flow universal characteristics are found in good agreement with previous theoretical, experimental and numerical studies. Some new results are shown in this study such as (i) the application of the Guo et al. forcing with the MRT model (Guo *et al.*, 2002) , (ii) comparison between the SRT and MRT simulations of forced turbulence and (iii)study the improvement of the incompressibility in favor of the MRT model. Some other issues are not addressed in this study and can be investigated in future work such as higher resolution simulations and parallelization and vectorization of the LBM models to reduce the simulations time as well as the data volume.

. Acknowledgement

"This project was supported financially by the Academy of Scientific Research and Technology (ASRT), Egypt, Grant no. 6477". Also, the first author would like to thank Science, Technology & Innovation Funding Authority (STDF)-Egypt for using the laboratory established by grant No. (25865) in simulating the case of 256^3-MRT model.

. References

Albernaz, D., Do-Quang, M., Hermanson, J. & **Amberg, G., (2016)**. Thermodynamics of a real fluid near the critical point in numerical simulations of isotropic turbulence. *Physics of Fluids*, **28**, 125105.

Albernaz, D., Do-Quang, M., Hermanson, J. & **Amberg, G., (2017)**. Droplet deformation and heat transfer in isotropic turbulence. *J. Fluid Mech.*, **820**, 61-85.

Bhatnagar, P., Gross, E. & **Krook, M., (1954)**. A Model for Collision Processes in Gases. I. Small Amplitude Processes in Charged and Neutral One-Component Systems. *Phy. Rev.*, **94**, 511-525.

Bouzidi, M., d'Humieres, D., Lallemand, P. & **Luo, L., (2001a)**. Lattice Boltzmann equation on a two-dimensional rectangular grid. *J. Computat. Phys.*, **172**, 704-717.

Buick, J. & **Greated, C., (2000)**. Gravity in a lattice Boltzmann model. *Phys. Rev. E*, **61(5)**, 5307-5320.

Comte-Bellot, G. & **Corrsin, S., (1971)**. Simple Eulerian time correlation of full and narrow-band velocity field signals in grid generated isotropic turbulence. *J. Fluid Mech.*,**48**, 273-337.

Cate, A. T., van Vliet, E., Derksen, J., Van den Akker, H., (2006). Application of spectral forcing in lattice-Boltzmann simulations of homogeneous turbulence. *Computers* & *Fluids.*, **35**, 1239-1251.

Courant, R. Friedrichs, K. & **Lewy, H., (1967)**. On the partial difference equations of mathematical physics, *IBM Journal of Research and Development*, **11**(2), 215–234.

Guo, Z., Zheng, C. & **Shi, B. (2022)**. Discrete lattice effects on the forcing term in the lattice Boltzmann method, *Phys. Rev. E*, **65**(046308), 1-6.

Haussmann, M., Simonis, S., Nirschil, H. & **Krause, M., (2019)**. Direct numerical simulation of decaying homogeneous isotropic turbulence-numerical experiments on stability, consistency and accuracy of distincit lattice Boltzmann methods. *Int. J. Mod. Phys. C.*, **30(9)**, 1950074.

Jiang, M., Li, J. & **Liu, Z., (2022)**. A simple and efficient parallel immersed boundary-lattice Boltzmann method for fully resolved simulations of incompressible settling suspensions, **Computers & Fluids**, **237**, 105322.

Kaneda, Y., Ishihara, T., Yokokawa, M., Itakura, K. & **Uno, A., (2003)**. Energy dissipation rate and energy spectrum in high resolution direct numerical simulations of turbulence in a periodic box. *Phys. of fluids*, **15**, L21-L24.

Kupershtokh, A., (2004). New method of incorporating a body force term into the lattice Boltzmann equation. *in Proceedings of the* 5^{th} *International EHD Workshop*, **4**, 241-246.

Lallemand, P., Luo, L.-S. & **Krafczyk, M., (2021)**. The Lattice Boltzmann Method for Nearly Incompressible Flows. *J. Comput. Phys.*, 109713.

Lu, J., Dai, C. & **Yu, P., (2022)**. Analysis and reconstruction of the simplified thermal lattice Boltzmann method. *International Journal of Heat and Mass Transfer*, **187**, 122576.

Aslan, E., Taymaz, I. & **Benim, A. C., (2014)**. Investigation of the Lattice Boltzmann SRT and MRT Stability for Lid Driven Cavity Flow. *International Journal of Materials, Mechanics and Manufacturing*, **2**, 317-324.doi:10.7763/IJMMM.2014.V2.149.

Ma, C., Wu, J., Yu, H. & **Yang, L., (2022)**. A high-order implicit-explicit flux reconstruction lattice Boltzmann method for viscous incompressible flows. **Comut. Math. Appl.**, **105**, 13-28.

Mohamad, A. & **Kuzmin, A., (2010)**. A critical evaluation of force term in lattice Boltzmann method, natural convection problem. *Int. J. Heat and Mass Transfer*, **53**, 990-996.

Ginzbourg I., & **Adler, P., (1994)**. Boundary flow condition analysis for the three-dimensional lattice Boltzmann model. *J. Physique II France*, **4**, 191-214.

Ladd, A., (1994). Numerical simulations of particulate suspensions via a discretized Boltzmann equaion. I. Theoretical foundation. *J. Fluid Mech.*, **271**, 285-309.

Giraud, L., d'Humieres, D. & **Lallemand, P., (1997)**. A lattice Boltzmann model for visco-elasticity. *Int. J. Mod. Phys. C*, **8**, 805-815.

Giraud, L., d'Humieres, D. & **Lallemand,P., (1997)**. A lattice Boltzmann model for Jeffreys viscoelastic fluid. *Europhys. Lett.*, **42**, 625-630.

d'Humieres, D., Bouzidi, M. & **Lallemand, P., (2001)**. Thirteen-velocity three-dimensional lattice Boltzmann model. *Phys. Rev. E*, **63**, 066702-1-7.

d'Humieres, D., Lallemand, P. & **Luo, L., (2002)**. 3D multiple relaxation time lattice Boltzmann equation models. *Phyil. Trans. R. Soc. Lond. A*, **61**, 437-451.

Valino, L., Martin, J. & **Hazi, G., (2010)**. Dynamics of isotropic homogeneous turbulence with linear forcing using a lattice Boltzmann method. *Flow Turbulence Combustion*, **84**, 219-237.

Hunt, J., Wray, A. & **Moin, P., (1988)**. Eddies, streams, and convergence zones in turbulent flows. *Report CTR-S88*, Center For Turbulence Research, 193-208.

d'Humieres, D., (1992). Generalized lattice Boltzmann equations. In rarefied gas dynamics: theory and simulations (ed. Shizgal, B. D. & Weaver, D. P.). *Prog. Aeronaut. Astronaut.*, **159**, 450-458.

Jimenez, J., Wray, A., Saffman, P. & **Rogallo, R., (1993)**. The structure of intense vorticity in isotropic turbulence. *J. Fluid Mech.*, **255**, 65-90.

Karlin, I., Asinari, P. & **Succi, S., (2011)**. Matrix lattice Boltzmann reloaded. *Phil. Trans. Roy. Soc. A*, **369**, 2202-2210.

Lallemand, P. & **Luo, L., (2000)**. Theory of the lattice Boltzmann method: dispersion, dissipation, isotropy, Galilean invariance and stability. textitPhys. Rev. E, **61**, 6546-6562.

Luo, L., (1993). Lattice gas automata and lattice Boltzmann equations for two-dimensional hydrodynamics. *PhD. thesis*, Georgia Institute of Technology.

Ooi, A., Martin, J., Soria, J. & **Chong, M., (1999)**. A study of the evolution and characteristics of the invariants of the velocity gradient tensor in isotropic turbulence. *J. Fluid Mech.*, **381**, 141-174.

Shan, X. & **Chen, S., (1994)**. Simulation of nonideal gases and gas-liquid phase transitions by the lattice Boltzmann equation. *Phys. Rev. E*, **49(4)**, 2941-2948.

Vincent, A. & **Meneguzzi, M., (1991)**. The spatial structures & statistical properties of homogeneous turbulence. *J. Fluid Mech.*, **225**, 1-20.

Kareem, W. A, Izawa, S., Xiong, A-K. & **Fukunishi, Y., (2006)**. Identification of multi-scale coherent eddy structures in a homogeneous isotropic turbulence. *Prog. Comput. Fluid Dyn.*, **6(7)**, 402-408.

Kareem, W. A., Izawa, S., Xiong, A-K. & **Fukunishi, Y., (2009)**. Lattice Boltzmann simulations of homogeneous isotropic turbulence. *Comp. Math. Appl.*, **57**, 1051-1061.

Kareem, W. A., (2020). A vortex identification method based on strain and enstrophy production invariants. *Int. J. Mod. Phys. C.*, **31**, 2050003.

Kareem, W. A. & **Asker, A., (2022)**. Simulations of isotropic turbulence using lattice Boltzmann method with different forcing functions. *Int. J. Mod. Phys. C.*, 2250145.

Kareem, M. A. & **Mohamed, H., (2022)**. Comparison between variable forcing techniques of the lattice Boltzmann method for turbulent flow simulations. *Progress in Comput. Fluid Dynamics.*, Accepted.

Yokokawa, M., Itakura, K., Uno, A., Ishihara, T. & **Y. Kaneda (2002)**. 16.4 Tflops direct numerical simulation of turbulence by a Fourier spectral method on the Earth Simulator. *in Proceedings of the ACM/IEEE 2002 Conference on Supercomputing*, 50.

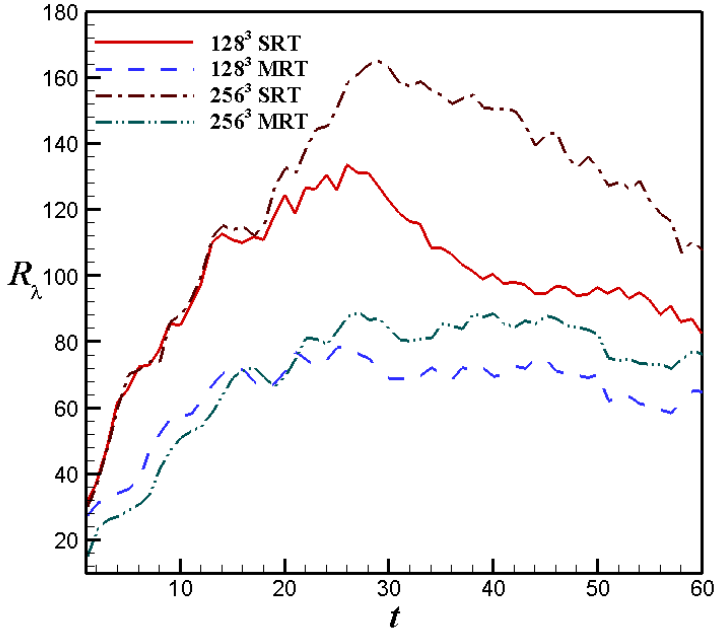

Fig. 1. SRT and MRT time-development of R_λ.

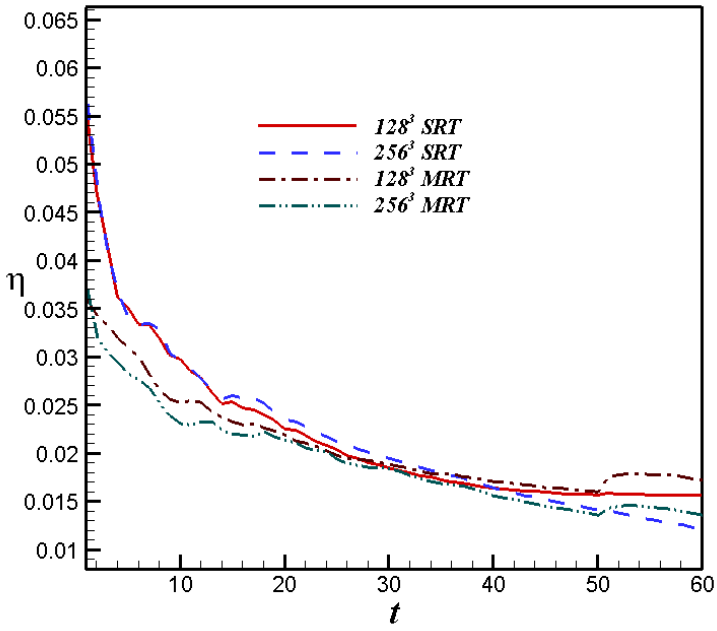

Fig. 2. SRT and MRT time-development of η.

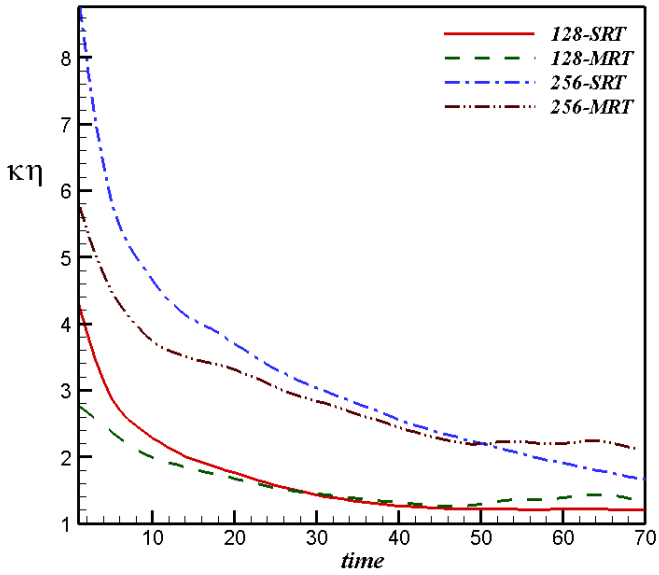

Fig. 3. SRT and MRT time-development of $k\eta$.

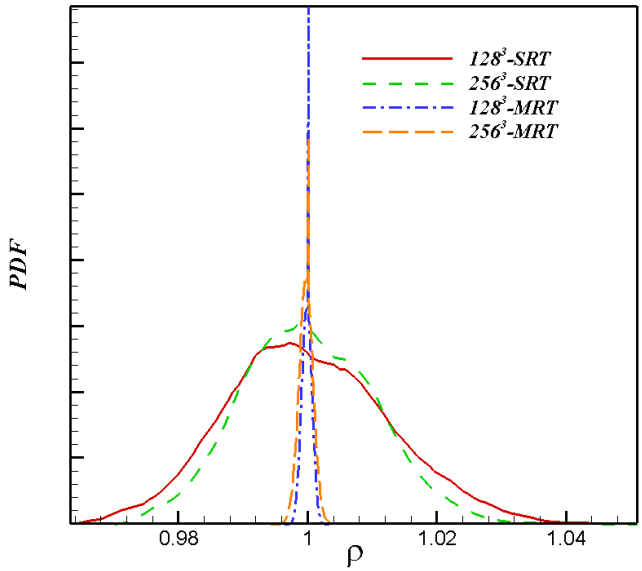

Fig. 4. SRT and MRT density PDF-profiles.

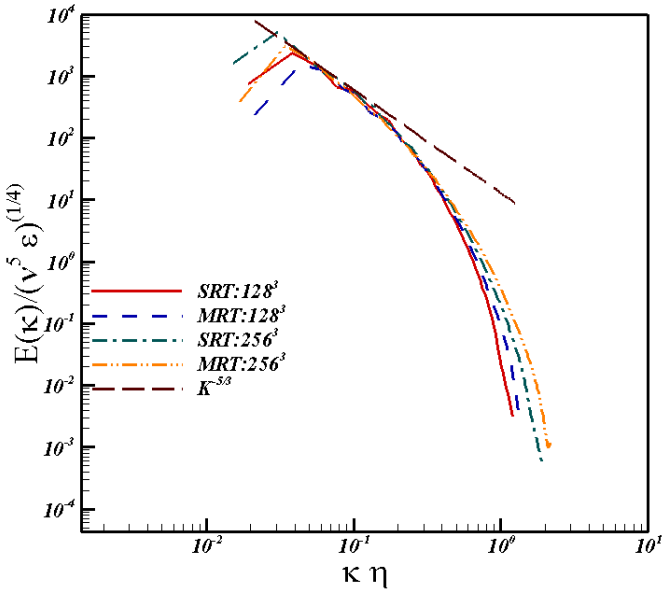

Fig. 5. SRT and MRT energy spectra.

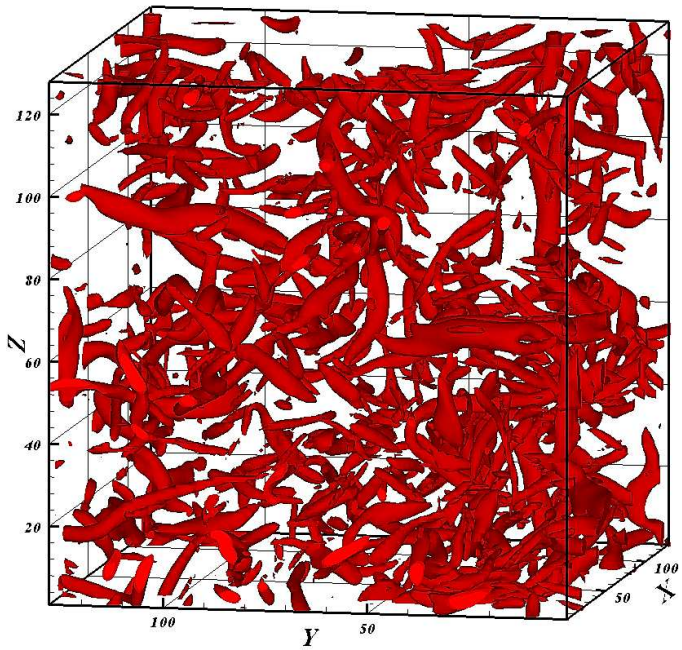

Fig. 6. Q-isosurfaces for 128^3-SRT case with $\frac{Q}{Q_w} = 5.0$

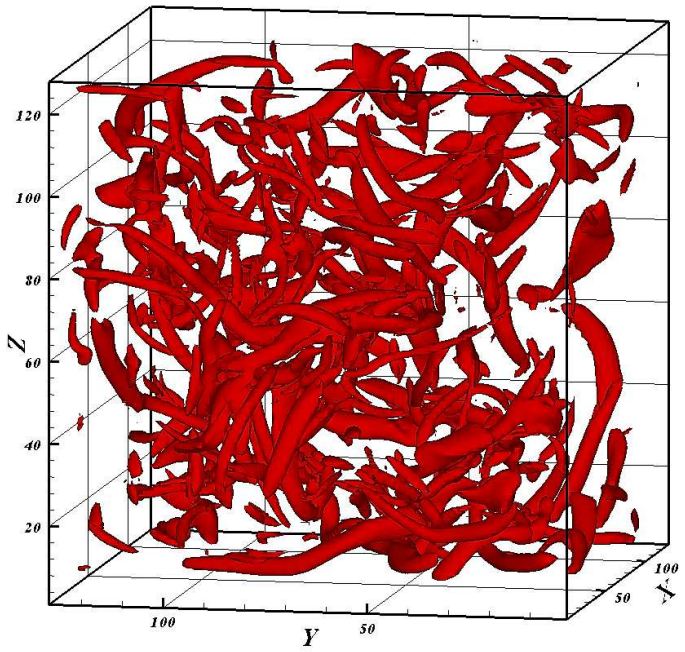

Fig. 7. Q-isosurfaces for 128^3-MRT case with $\frac{Q}{Q_w} = 5.0$

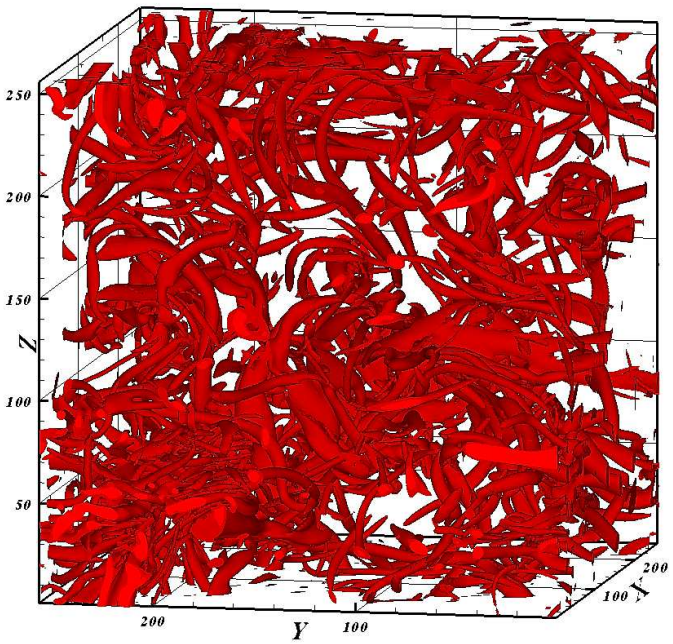

Fig. 8. Q-isosurfaces for 256^3-SRT case with $\frac{Q}{Q_w} = 5.0$

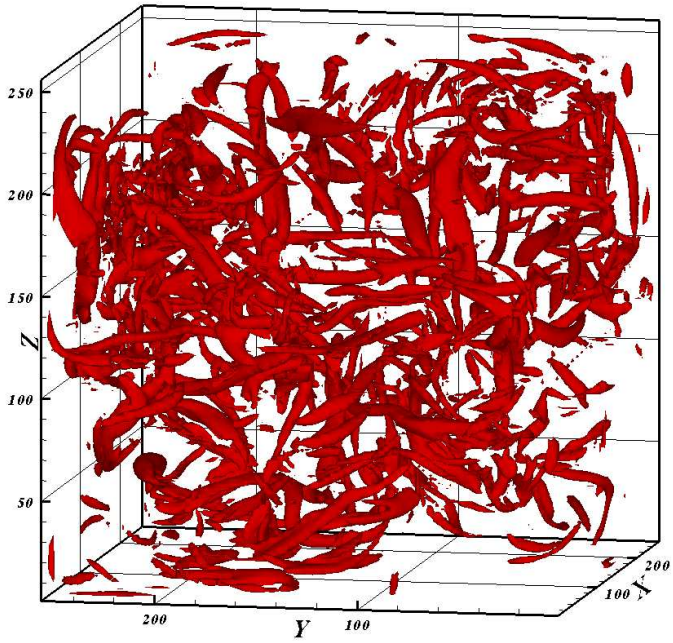

Fig. 9. Q-isosurfaces for 256^3-MRT case with $\frac{Q}{Q_w} = 5.0$

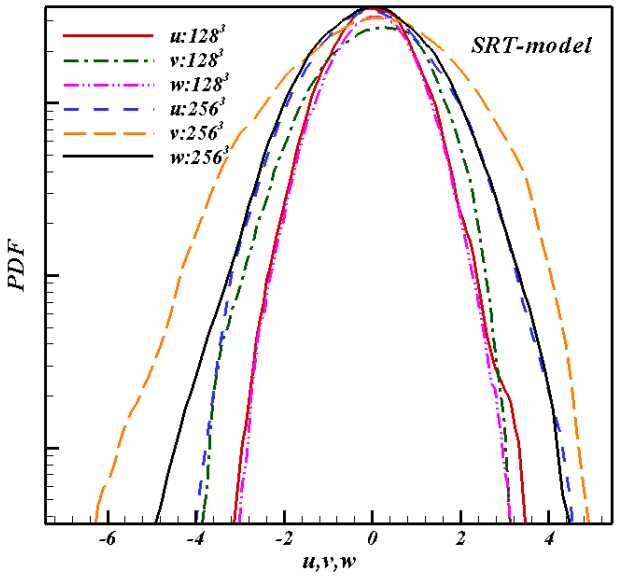

Fig. 10. PDFs of SRT velocity components.

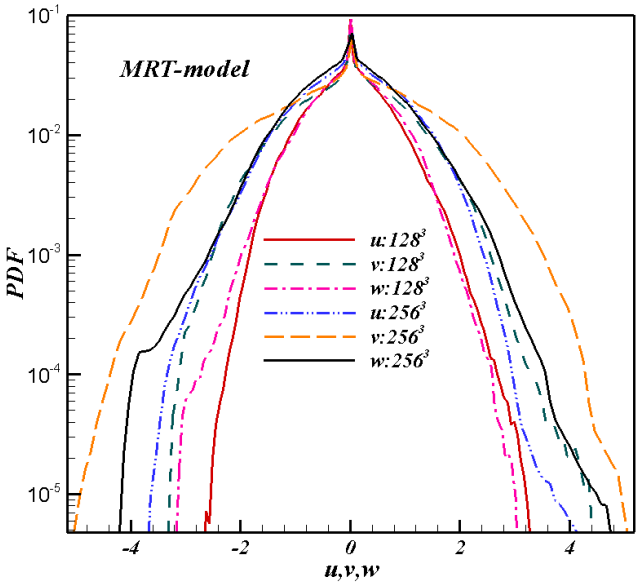

Fig. 11. PDFs of MRT velocity components.